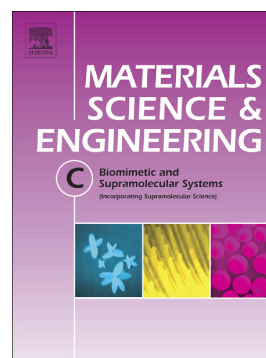# Accepted Manuscript

Chitosan and polyethylene glycol based membranes with antibacterial properties for tissue regeneration

Inês C. Pereira, Ana S. Duarte, Ana S. Neto, J.M.F. Ferreira

Chitosan and Polyethylene glycol based membranes with antibacterial properties for tissue regeneration

Inês C. Pereira [a], Ana S. Duarte [b], Ana S. Neto [a], J.M.F. Ferreira [a,*]

[a] *Department of Materials and Ceramics Engineering, University of Aveiro, CICECO, Aveiro 3810-193, Portugal*

[b] *Department of Biology, University of Aveiro, CESAM, Aveiro 3810-193, Portugal*

Keywords:

Composite membranes

Calcium phosphates

Zinc oxide

Copper oxide

Antimicrobial activity

Biocompatibility

* Corresponding author

E-mail address: jmf@ua.pt

Abstract

The prevention of microbial infections associated with implantable medical devices and superficial wounds represents one of the main research strategies in the field of biomaterials. The present study reports on the development of composite membranes of Chitosan (CS)−Polyethylene glycol (PEG) matrix, incorporating particles of biphasic calcium phosphate (BCP), zinc oxide (ZnO) and copper oxide (CuO). The properties that are relevant for intended applications in tissue regeneration and antibacterial coatings of implants were assessed. It was found that the addition of 1 % (w/w - relative to the mass of CS) of each metal oxide promoted satisfactory bacteriostatic activity and exhibited no cytotoxic effects towards the Vero cell line. The formation of bonds between the CS/PEG matrix and ionic species from the powders enhanced the cross-linking degree and mechanical properties of composite membranes in comparison to the non-doped membrane with the same polymer matrix (CS/PEG=70/30 %). A gradual degradation of the composite membranes over the immersion time in simulated body fluid (SBF) was accompanied by a continuous surface deposition of uniform apatite layer.

1.   Introduction

The development of biomaterials with antimicrobial properties for tissue engineering applications has become a primary strategy for prevention of infections associated with medical devices [1]. These infections, caused by the local colonization of pathogenic microorganisms and by the formation of bacterial biofilms, could lead to premature implant removal and replacement, among other complications [2]. One way to overcome these problems involves the design of implant coatings capable of preventing the bacterial adhesion and proliferation [3,4]. Furthermore, it is an added value if the systems developed are able to promote the regeneration of damaged tissues [5].

Chitosan (CS) [poly-β(1→4)-2-amino-2-deoxy-D-glucose] is a natural cationic amino polysaccharide derived from partial deacetylation of chitin, one of the most abundant natural polysaccharide. Chitin is extracted from the exoskeleton of crustaceans and insects, and from fungal cell walls [6,7]. CS has been receiving much attention in various fields of biomedicine due to its remarkable properties, like biodegradability, biocompatibility and non-toxicity [8]. It can be molded in a wide variety of forms, such as scaffolds, fibers, membranes, sponges, hydrogels and nanoparticles, which allows its use in numerous applications, like in controlled drug delivery systems, antibacterial coatings, bone regeneration, and so one [9,10].

Despite the excellent properties of CS, membranes only formed by this material are fragile and brittle, with poor mechanical strength and flexibility. Among the strategies used to improve CS mechanical properties, polyethylene glycol (PEG) cross-linked CS has been proved to present better mechanical features than individual CS [11–14]. PEG is a synthetic polymer approved by the food and drug administration (FDA, USA) for drug delivery systems and internal consumption. It is a hydrophilic, plasticizer, biocompatible, non-toxic, non-immunogenic and

non-inflammatory polymer. These unique properties make this polymer ideal for blending with CS [15].

As the main inorganic part of bone, calcium phosphates have been widely used in bone tissue engineering applications [16]. Among the different phases of calcium phosphates, hydroxyapatite (HAp) and β-tricalcium phosphate (β-TCP) have been the most applied in biomedicine due to their good solubility in human body. In fact, an appropriate proportion between these two materials – biphasic calcium phosphates (BCP) – can provide reabsorption rates suitable for bio-ceramic applications [17,18]. In order to improve bioactivity of chitosan based materials for bone regeneration, various studies have been reporting the incorporation of BCP particles into various chitosan forms [16,19–23]. Also, it was already proved that calcium phosphates promote angiogenesis, and Ca^{2+} cations promote the regulation of skin homeostasis, which make BCP-doped chitosan membranes potential materials for application in regeneration of other damaged tissues, such as skin [24].

For improving antibacterial activity of chitosan based materials, chitosan has also been complexed with metal or metal oxide particles [13,14,25–27]. Among the metals commonly used, copper and zinc oxides present relevant advantages: (i) are cheaper and less toxic than silver and gold, for example [28]; (ii) copper promotes angiogenesis [29]; (iii) zinc promotes osteogenesis and wound healing [30,31]; and (iv) a synergic antibacterial action is reached when both materials are combined [26,32,33].

Considering the importance of all materials mentioned, the present study reports on the development of a composite membrane of CS/PEG matrix incorporating particles of BCP, copper oxide (CuO) and zinc oxide (ZnO). The powders synthesized *ex situ* by hydrothermal treatment, were characterized by XRD, FTIR and SEM. Antimicrobial properties and cytotoxicity of the composite membranes with different contents of CuO and ZnO were

evaluated. The mechanical behavior of the selected membrane composition, and their biodegradation, biomineralization and chemical nature are reported.

2.   Materials and Methods

2.1. Materials

Calcium nitrate tetrahydrate (Panreac), di-ammonium hydrogen phosphate (Panreac), zinc nitrate hexahydrate (Sigma-Aldrich), copper nitrate trihydrate (Honeywell Fluka™), urea (Riedel-de Haën), chitosan (medium molecular weight = 190 − 310 kDa, 75 − 85 % deacetylation, Sigma-Aldrich) and polyethylene glycol (MW = 10 000 g mol^{-1}, Sigma-Aldrich) were purchased and utilized without further purification. For antibacterial and cytotoxic assays, plate count agar and tryptic soy broth were obtained from Merck; Dulbecco's Modified Eagle Medium (DMEM), phosphate buffered saline (PBS), trypsin and fetal bovine serum (FBS) were purchased from Thermo Fisher Scientific and resazurin from Sigma-Aldrich. The reagents used for simulated body fluid (SBF) preparation were obtained from Sigma-Aldrich. Sodium hydroxide, acetic acid and all other reagents were analytical grade.

2.2. Powder Synthesis

BCP, ZnO and CuO powders were produced via hydrothermal synthesis using urea as the precipitating agent. For the production of BCP powder, a Ca/P molar ratio of 1.55 was chosen in order to obtain a biphasic material. For that, two solutions were prepared separately: one containing Ca^{2+} precursor, $Ca(NO_3)_2 \cdot 4H_2O$; and another one containing 0.5 M of urea $[CO(NH_2)_2]$ and PO_4^{3-} precursor, $(NH_4)_2HPO_4$. After total dissolution of the individual prepared solutions, they were mixed together by stirring at room temperature for 15 min. The resultant mixture was transferred to a Teflon-lined stainless-steel autoclave and kept at 150 °C for 4 h. The white precipitate obtained was oven dried at 100 °C, and thereafter was calcined at 800 °C

for 2 h, with a heating rate of 3 °C minute^{-1} [34]. For the preparation of ZnO and CuO powders the precursors used were $N_2O_6Zn \cdot 6H_2O$ and $CuN_2O_6 \cdot 3H_2O$, respectively. The molar ratio of urea to metal ions was maintained at 2:1, for each metal oxide synthesis [35,36]. The solutions prepared underwent to the same hydrothermal treatment applied to BCP powder, and afterwards they were calcined in a furnace at 500 °C for 2 h [37], with a heating rate of 2 °C minute^{-1}. A brief illustration of powder synthesis is presented in **Fig. 1**.
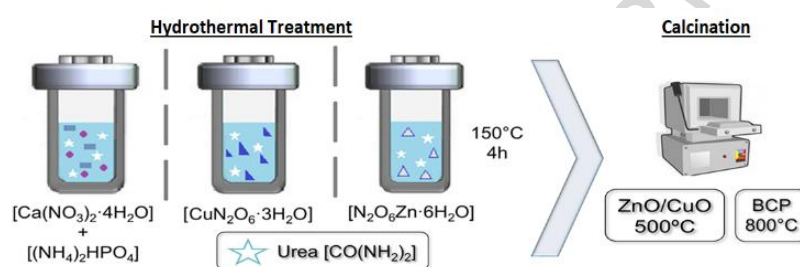

Fig. 1. Schematic illustration of powder synthesis process.

2.3. Powder characterization

X-ray diffraction (XRD) patterns of the synthesized powders were registered by a high-resolution X-ray diffractometer Rigaku Geigerflex D/Max-Serie C equipped with CuKα radiation (λ = 1.54056 Å). Crystalline phases determination was possible by using the Standard ICDD (International Centre for Diffraction Data) powder diffraction files (PDF) no. 04-015-7245 for HAp, 04-006-9376 for β-TCP, 01-078-2585 for ZnO, and 04-005-4712 for CuO. Semi-quantitative analysis of phases present in powders was done by the HighScore Plus Xpert-pro PANanalytical software associated to XRD equipment. Fourier transform infrared (FTIR) spectra of the powders was recorded by a Bruker (Tensor 27) spectrophotometer with a resolution of 4 cm^{-1}, using the KBr disc technique. The powders morphology was observed by scanning electron microscopy (SEM) using a Hitachi S-4100 (Japan) microscope.

2.4. Preparation of composite membranes

CS/PEG membranes reinforced with BCP, CuO and ZnO powders were produced by the solvent casting method. Through preliminary mechanical tests it was found that polymeric ratio of CS/PEG = 70/30 % presents better mechanical properties compared to other matrix compositions tested. Therefore, this polymeric proportion was used to produce the composite films. CS solution was prepared by dissolving 2 % (w/v) of CS powder in 2 % (v/v) of acetic acid solution under magnetic stirring (700 rpm) at room temperature (RT) for 2 h. The viscous solution was filtered to remove any undissolved particles, and thereafter mixed with a desired amount of PEG. The mixture was magnetically stirred for 1 h (700 rpm) at RT.

All the composite membranes contain a fixed amount of 35 % (w/w) of BCP relative to CS mass per membrane [16]. The following percentages of each metal oxide (CuO and ZnO): 0 %, 0.5 %, 1 %, 1.5 % and 2 % (w/w), relative to CS mass per membrane were added. To incorporate the inorganic powders into CS/PEG matrix, the required amount of each powder was weighted, dispersed in ethanol for 5 minutes using an ultrasounds bath, and then added to CS/PEG. The composite mixture was homogenized with a mixer (Thinky ARE-250) for 2 minutes at 900 rpm, and then poured into molds of different sizes and shapes depending on the test to be performed: for antibacterial and cytotoxic assays, ATR-FTIR analysis and SBF test, 12 well plates were used to minimize material waste; for mechanical tests, the solutions were poured into acrylic boxes with desired dimensions. The composite solutions were left at RT for one day to remove air bubbles, and then placed in an oven at 40 °C until solid membranes were obtained. For neutralization, the dry films were immersed in 1 M NaOH for 24 h, and then washed thoroughly with distilled water.

2.5. Biological tests

The most promising contents of ZnO and CuO to be incorporated into the composite

membranes were determined by antibacterial and cytotoxic assays. The added concentrations of metal oxides to achieve antibacterial properties and, at the same time, biocompatibility, were selected based on relevant data reported in previous research works [38–43]. Therefore, the six different membrane compositions named by: CS/PEG, 0 %, 0.5 %, 1 %, 1.5 % and 2 % (w/w) – mass percentage of each metal oxide added, relative to CS mass per membrane were compared.

2.5.1. Antibacterial assays

The antibacterial assays were performed according to the standard ASTM E2149 – 10 protocol [44], with some modifications. The materials – CS/PEG, 0 %, 0.5 %, 1 %, 1.5 % and 2 % – were tested against two types of bacteria: Gram-negative *Escherichia coli* (ATCC 25922) and Gram-positive *Staphylococcus aureus* (ATCC 25923). For both antibacterial tests (*E. coli* and *S. aureus*) microtubes with a bacterial suspension of 3×10^8 CFU mL^{-1} each were prepared. The membranes were then transferred to the respective test tubes and incubated at RT on an orbital shaker, for 1 h. A test tube without material was used as control. After finishing the dynamic contact time, 0.1 mL of each sample was used to prepare decimal dilutions that were spread in triplicates on nutrient agar plates. The inoculated plates were incubated at 37 °C for 24 h. The colonies were counted and the percentage of reduction of bacterial viability was calculated with respect to control (considering the dilution factor).

2.5.2. Cytotoxicity assay

The *in vitro* cytotoxicity of the different membrane compositions produced was evaluated according to the standard ISO 10993-5 protocol [45]. The Vero cell line (ECACC 88020401, African Green Monkey Kidney cells, CCL 81 clone) was grown and maintained according to *Ammerman et al.* [46]. Confluent cells were trypsinized and seeded into 12 well plates at a density of 1×10^5 cells/well and incubated for 24 h at 37 ºC with 5 % CO_2. The materials were

sterilized by UV radiation for 30 min and then added to the respective wells. Positive control (C^+) was not exposed to any material. After an incubation period of 24 h in the same conditions, the cytotoxic effects were determined by the Resazurin assay; the growth medium was aspirated and replaced with fresh DMEM, 5% FBS supplemented with 10 % resazurin (0.1 mg mL^{-1} in PBS) and incubated at 37 ℃ for 3h, to provide enough time for the reduction of resazurin to resorufin by viable cells metabolism. Resarurin was also added to an empty well (negative control, C^-). The content of wells was then removed and transferred to another microplate, and the absorbance was measured at 570 nm and 600 nm by a microplate reader (Multiskan Spectrum Microplate spectrophotometer, Thermo Scientific). All the experiments were performed in triplicate. Percentage of cell viability was calculated with respect to controls as follows:

$$\% \text{ cell viability} = \frac{(A_{570}/A_{600})_S - (A_{570}/A_{600})_{C^-}}{(A_{570}/A_{600})_{C^+} - (A_{570}/A_{600})_{C^-}} \times 100 \qquad (1)$$

where *A* represents the measured absorbance at 570 or 600 nm wavelengths, *S* corresponds to the sample (membrane compositions) and C^+/C^-, the positive/negative controls.

2.6. Characterization of composite membranes

Membranes doped with ZnO and CuO contents that did not induce any toxicity towards Vero cells and was capable of reduce the bacterial growth of *E. coli* and *S. aureus*, were characterized by different techniques.

2.6.1. ATR-FTIR analysis

The powders (BCP, CuO and ZnO) and three membrane samples – one uniquely formed by CS, another consisting of CS/PEG matrix, and a selected composite – were analyzed by FTIR

using a Bruker (Tensor 27) spectrophotometer in attenuated total reflectance (ATR) mode, by using a Golden Gate (Diamond, SPECAC) accessory. ATR-FTIR technique was adopted because it allows infrared spectra to be obtained from difficult-to-dust samples as the membranes here developed, which hardily could be molded into KBr pellets.

2.6.2. Mechanical properties

Tensile strength and elongation at break of composite membranes were evaluated. The mechanical test was performed according to standard ASTM D 882 – 02 protocol [47], by using a tensile testing machine (Shimadzu Autograph, Japan, equipped with the software Trapezium) with a crosshead speed of 50 mm min^{-1} and a 5 kN static load cell. The membranes were cut into specimens with a dimension of 100 x 20 x 0.25 mm (length x width x thickness), and at least five samples of the composite film and CS/PEG film (for comparing) were tested. The test was performed with the samples slightly moist to better reproduce the mechanical properties of the materials in human body. Tensile strength at break was calculated by dividing the maximum load at break by the original minimum cross-sectional area of the specimen. Percent elongation at break was calculated by dividing the extension at the moment of rupture of the specimen by the initial gage length of the specimen, and multiplying by 100.

2.6.3. In vitro bioactivity study

To evaluate the biodegradability and biomineralization ability of the composite membrane, a SBF test was performed according to standard ISO 23317:2014(E) protocol [48], but using the unifying standard area (S_A) of 0.5 cm^2 m^{-1} of SBF recently proposed [49]. Membrane samples of 1 cm in diameter were prepared and soaked in SBF solution at 37 °C for 0, 3, 7 and 14 days. After each immersion time, the samples were taken out, rinsed with deionized water and placed in a silica desiccator. The morphology of the membranes was then observed by scanning electron

microscopy (SEM) using a Hitachi S-4100 (Japan) microscope.

2.7. Statistical analysis

Data representative of at least three independent experiments are expressed as the mean $\pm$ the standard deviation (SD) and analyzed using one-way ANOVA or Welch's *t*-test, where for $p < 0.05$ the differences were considered statistically significant.

3.   Results and Discussion

3.1. Powder characterization

Crystalline phases of the different powders produced were identified by XRD technique (**Fig. 2a**). For of BCP powder, the two highest diffraction peaks at 2θ = (31.78º and 32.92º) correspond to HAp with hexagonal crystalline structure, and the following peaks at 2θ = (27.82º, 31.03º and 34.40º) confirm the presence of β-TCP with rhombohedral configuration. The semi-quantitative percent of these two phases was successfully estimated by the software associated to XRD equipment, which confirmed the presence of 52 % HAp and 48 % β-TCP.
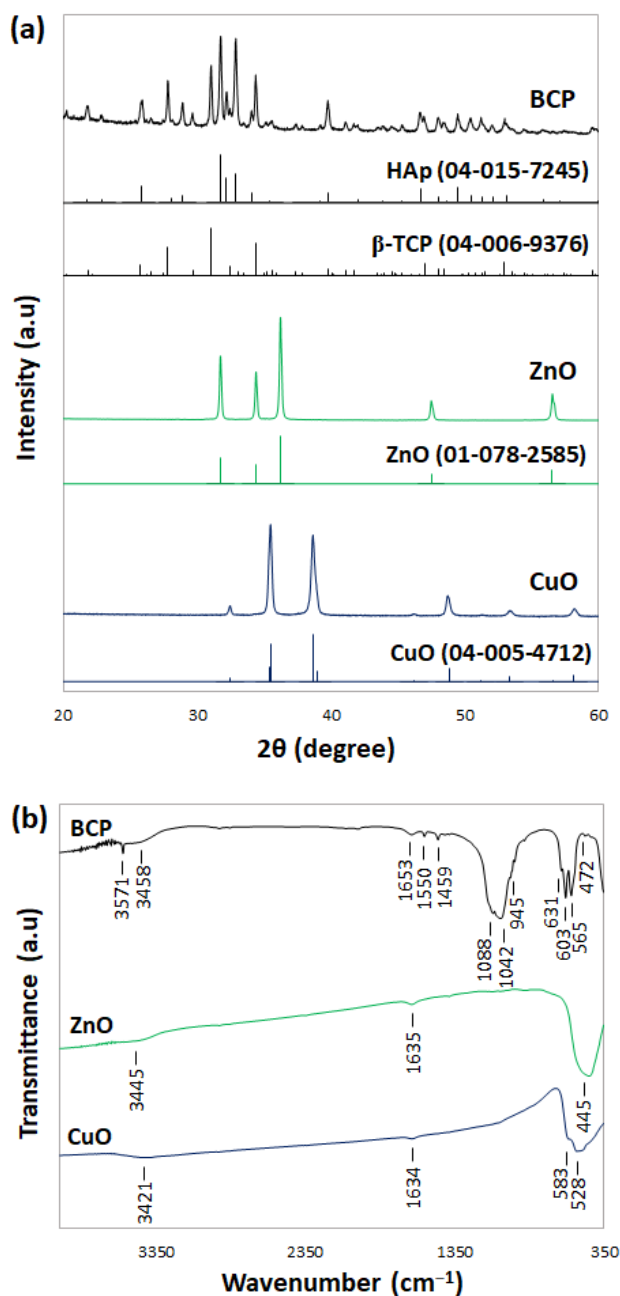
Fig. 2. (a) XRD pattern and (b) FTIR spectra of BCP, ZnO and CuO powders.

The BCP powder composition presents an optimum combination that benefits a good balance between reabsorption rates and new bone formation [5]. The diffraction patterns of metal oxides confirm their high levels of purity and crystallinity: ZnO with hexagonal crystalline structure (wurtzite) and CuO with monoclinic configuration.

FTIR spectra of powders are present in **Fig. 2b**. For BCP, the adsorption peaks at 3458 and

631 cm^{-1} correspond to the vibrational modes of OH group that is due to the existence of HAp phase. PO_4^{3-} groups present vibrational bands at 1088, 1042, 945, 603, 565 and 472 cm^{-1}. The low intensity peaks at 1550 and 1459 cm^{-1} are assigned to A-type carbonation in HAp (substitution of CO_3^{2-} for OH$^-$ ions), that is not problematic since carbonate ions are also present in natural bone. The relatively broad band at 3571, and the peak at 1653 cm^{-1}, are due to the presence of water adsorbed by the powder [19,50,51]. In FTIR spectrum of ZnO it is possible to identify the presence of a highly intense adsorption peak at 445 cm^{-1} that is attributed to the vibration of Zn–O bond [52]. For CuO powder, the bands correspondent to Cu–O bond vibration can be observed at 583 and 528 cm^{-1} [53]. The remaining peaks in the FTIR spectra of both ZnO and CuO are associated to the water adsorbed by the samples. XRD and FTIR analysis make it possible to conclude that highly pure powders were successfully produced via urea-assisted hydrothermal treatment.

SEM images of BCP, ZnO and CuO particles are shown in **Fig. 3**. It can be seen that the materials synthesized are formed by particles with nanometric dimensions that cluster during the synthesis and processing originating some large agglomerates. This agglomeration occurs because the newly formed nanoparticles present a high surface-to-volume ratio, which results in high colloidal instability due to the high ionic strength of the reaction medium and the predominance of the attractive Van der Walls forces among the particles. Despite the presence of agglomerates, the powders present particle sizes that are acceptable for the application.
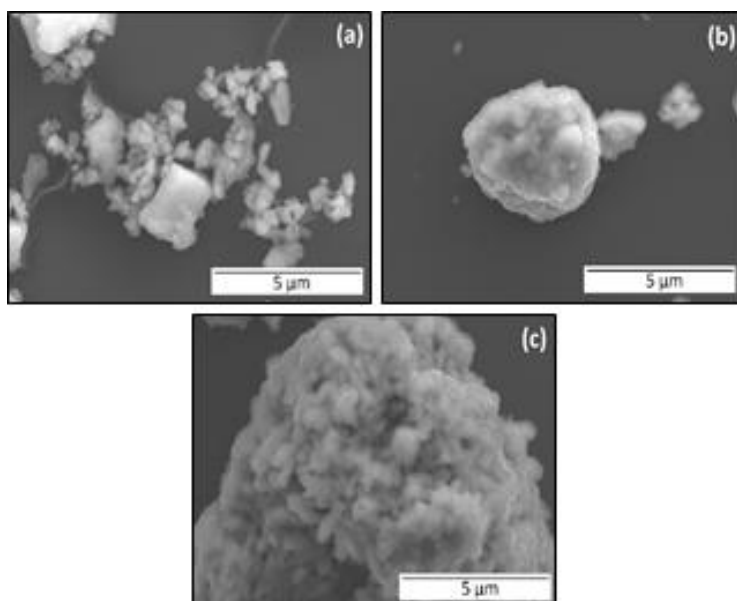
Fig. 3. SEM images of (a) BCP, (b) ZnO, and (c) CuO particles.

3.2. Biological tests

3.2.1. Antibacterial activity

Different amounts of metal oxides were added to CS/PEG membranes (0 %, 0.5 %, 1 %, 1.5 % and 2 %) and their antibacterial properties against Gram-positive bacteria *S. aureus* and Gram-negative bacteria *E. coli* were accessed by plate counting method. The results obtained are given in **Fig. 4**.
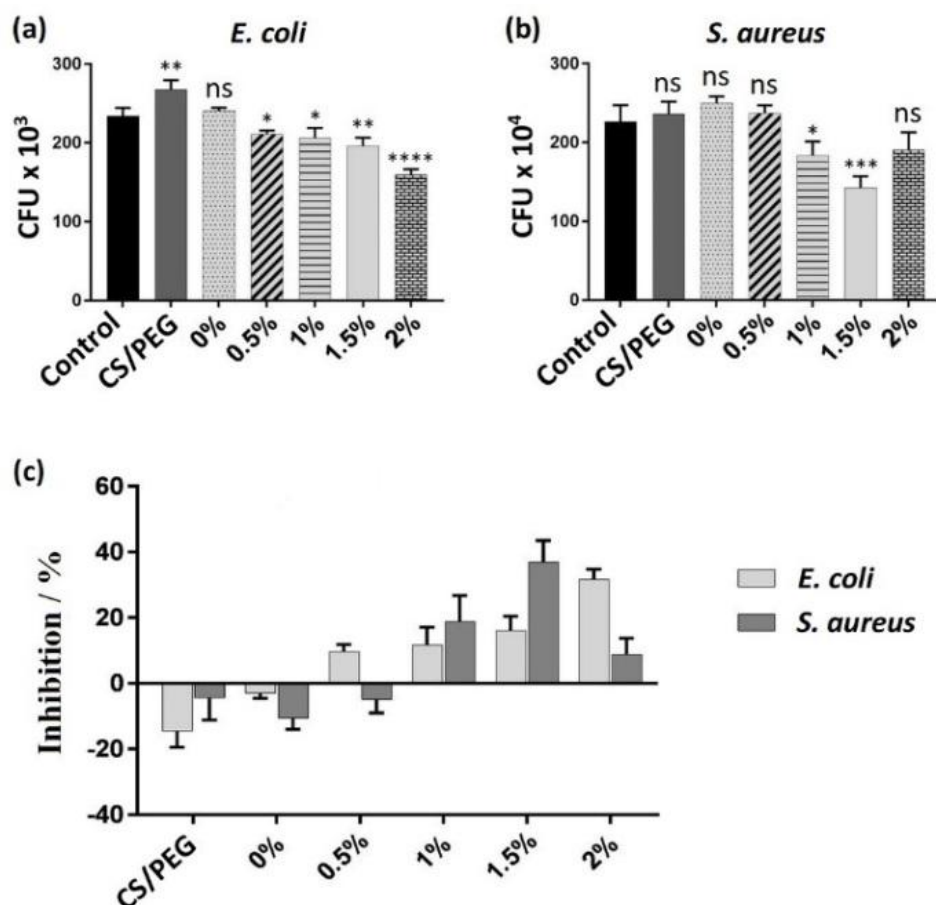
Fig. 4. Evaluation of antibacterial activities of different membrane compositions (ASTM E2149 – 10 protocol). Number of (a) *E. coli* and (b) *S. aureus* CFU mL^{-1}; (c) Growth inhibition of *E. coli* and *S. aureus* promoted by the membranes: CS/PEG, and BCP-doped CS/PEG membrane 0 %, 0.5 %, 1 %, 1.5 % and 2 % (w/w) – mass percentage of each metal oxide added, relative to CS mass per membrane. The data represents the mean ± SD (n = 3). *, **, *** and **** represent $p \leq 0.05$, $p \leq 0.01$, $p \leq 0.001$ and $p \leq 0.0001$, respectively. "ns" represents a difference non-statistically significant.

Observing the data, it is possible to verify that CS/PEG membrane do not present any toxicity towards two types of bacteria tested. This fact can be attributed to the well-succeeded membrane neutralization. CS is capable of inhibit bacterial viability through the electrostatic interaction

between its protonated amine groups NH_3^+ and negative charges on the microbial cell surface. With the neutralization process, protonated terminals are neutralized to NH_2, which do not present any negative action against bacteria [54]. The absence of antibacterial properties is verified as well in BCP-doped CS/PEG membrane (0 %), which was expected since BCP is a non-toxic material. On the other hand, with slightly increasing concentrations of metal oxides incorporated into the composite, the reduction of CFU for both bacteria is notable. Antibacterial properties of metal oxides are widely reported in literature, where the main proposed antibacterial mechanisms are the production of reactive oxygen species (ROS) and the release of metal ions [55]. The toxicity of these species involves its internalization into the bacteria cell membrane, which leads to the destruction of cellular components such as lipids, DNA and proteins that can trigger cell death. For the possible applications of the developed composite, such as a coating material for implants, in protection of superficial wounds, or even in separating soft and hard tissues (for example in dental medicine surgeries), the main objective is not to achieve an absolute bacterial reduction (bactericidal action), but instead a reduction in bacterial growth (bacteriostatic action). That is, membranes must present antibacterial properties for preventing biofilm formation and microbial proliferation, without causing a significant change in the balance between commensal and pathogenic microorganisms. So, it can be concluded that 1 % and 1.5 % compositions give a suitable antibacterial action to the membranes in the scope of their intended applications.

For these membrane compositions, it is also possible to verify that Gram-positive bacteria *S. aureus* is more susceptible to the composite than Gram-negative bacteria *E. coli*. This result is in accordance with some reported studies [26,27], and may be related with the different cell wall compositions of these two types of bacteria: the cell wall of Gram-positive bacteria is essentially composed by a thick layer of peptidoglycan, which contains in abundance amide, carboxyl and hydroxyl groups, and also teichoic and lipoteichoic acids; Gram-negative bacteria cell wall is

more complex due to the presence of an additional external membrane, and a thin layer of peptidoglycan, phospholipids, lipoproteins, lipopolysaccharides and proteins [56]. The complexity of *E. coli* cell wall makes it more resistant to the action of ROS and metal ions. On the other hand, is proposed in the literature that metal ions have affinity for functional groups present on Gram-positive bacteria cell wall, which can explain the more susceptibility of *S. aureus* to the material [57].

We can also verify that 2% (w/w) of ZnO and CuO displays a lower effect on growth inhibition of *S. aureus*. In fact, the growth inhibition of S. aureus in response to 2.0% (w/w) of metal oxides is significantly lower to that expressed by E. coli. Nevertheless, this result is not so surprising and may be related, not only to the known different stress response mechanisms by Gram negative and Gram positive microorganisms, but also to transcriptional regulation events that are often modulated by the concentration of potentially toxic substances. A variety of multi-drug pumps are encoded by some Gram-positive organisms including *S. aureus*. In addition to multi-drug efflux pumps that actively expel a broad range of unrelated and structurally diverse compounds [58,59], there are also efflux pumps that expel metal ions [60]. Efflux pumps expression is usually under transcriptional regulation by DNA-binding factors of activator and repressor genes. Transcriptional factors may be upregulated by substrates or bind them directly, thereby providing routes by which efflux activity may be modulated according to the increasing metal concentration [60]. This strategy protects the bacteria from expending energy on indiscriminate extrusion of metabolically useful molecules when toxic compounds are not present or when bacteria is exposed to sub-inhibitory concentrations. This helps explaining the reversion of *S. aureus* response to the increase of ZnO and CuO concentration (2 %).

3.2.2. Cytotoxicity

Cytotoxicity of the non-doped and doped membranes was evaluated based on the analysis of viability of Vero cells after 24 h of contact with the materials. **Fig. 5** shows the results obtained, where it is possible to verify that the percentage of viable cells decreased with the increasing concentrations of metal oxides, and no cytotoxic effect was observed up to 1.5 % by weight of each metal oxide added to the membranes (% cell viability $\geq$ 70 %).
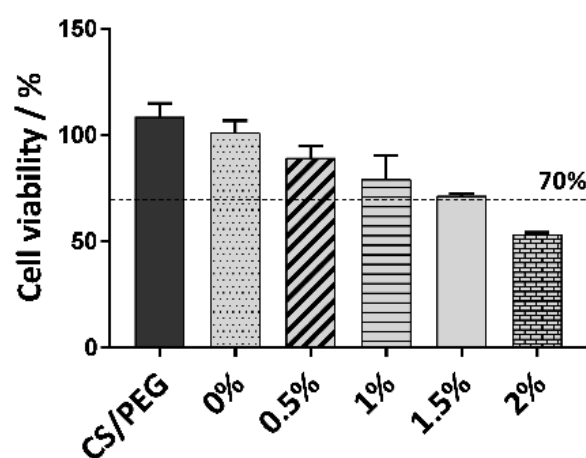

Fig. 5. Viability of Vero cells exposed to the different composite membranes: CS/PEG and 0 %, 0.5 %, 1 %, 1.5 % and 2 % (the different amounts of metal oxides added to BCP-doped CS/PEG membranes). The dashed line denotes the acceptable criteria of 70 % cell viability (ISO 10993-5) [45]. The data represents the mean $\pm$ SD (n = 3).

Considering the results of antibacterial tests, it can be concluded that membranes incorporated with 1 % to 1.5 % (w/w) of each ZnO and CuO can promote a satisfactory growth inhibition of *E. coli* and *S. aureus* without inducing any cytotoxic effect. Therefore, 1 % composition was chosen to carry out the following tests as it corresponds to the minimum inhibitory concentration.

3.3. Membrane properties

3.3.1. ATR-FTIR analysis

Membranes of CS, CS/PEG matrix, and of a composite one incorporating 1% (w/w) of each inorganic powder were analyzed by ATR-FTIR technique. The spectra of CS and CS/PEG membranes are compared in **Fig. 6** in order to infer about the chemical interactions between the two polymers.

The ATR-FTIR spectrum of CS exhibits typical absorption bands of CS biopolymer: in the blue-colored region, the broad peak around 3315 cm^{-1} is assigned to the overlapping of O–H stretching and N–H stretching bands, and the peak at 2880 cm^{-1} is due to the aliphatic C–H stretching; in the pink-colored region, between 1170 – 1710 cm^{-1} are present the absorption bands of CS amide groups (I, II and III), where the two peaks at 1646 and 1572 cm^{-1} are respectively assigned to C=O bending (–NHCO– group, amide I) and N–H stretching vibration (–NH$_2$ group, amide II); finally, in the green-colored region is displayed a strong band between 1102 – 917 cm^{-1} that represents the skeletal vibrations of the CS saccharide structure.
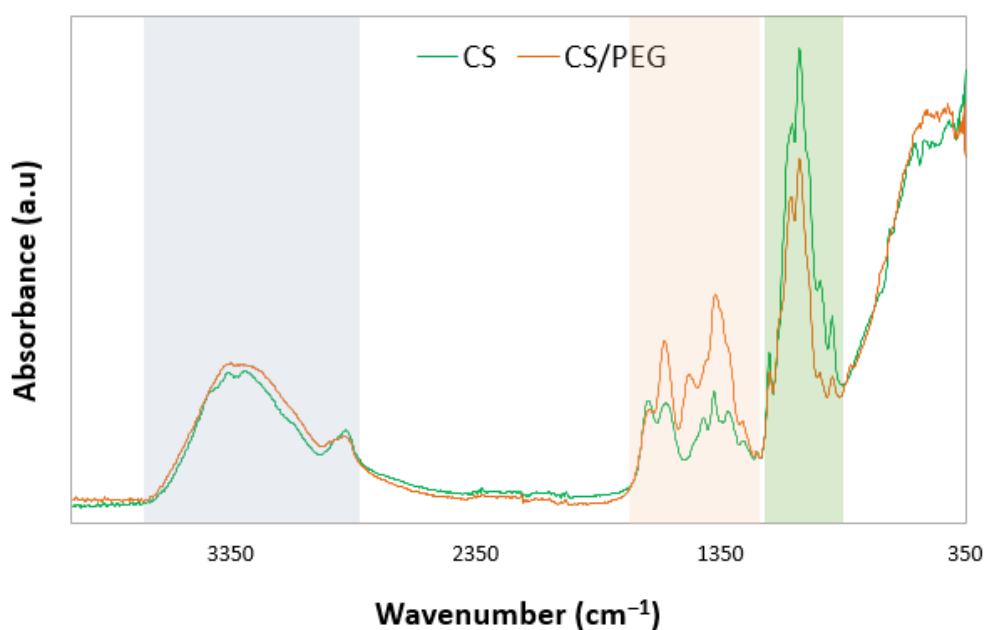

Fig. 6. ATR-FTIR spectra of CS and CS/PEG membranes.

Comparing CS and CS/PEG spectra, significant differences can be observed in the pink- and the green-colored regions. In the first one, the addition of PEG has strengthened almost all peaks corresponding to bending vibrations of amide groups, except the peak corresponding to C=O stretching vibration that slightly decreased. The change in amide bands may indicate that CS interacts with PEG essentially through hydrogen bonds that are formed between PEG hydroxyl groups and CS amine portions. These bonds can alter the vibration of amide groups, explaining the deformations in amide absorption bands. The shift in C=O peak towards lower intensities can be due to additional interactions that may exist between this CS portion and the hydroxyl groups of PEG as reported by *Du, Jian & Hsieh, You Lo* [61]. All these intramolecular interactions can therefore explain the changes verified in the CS saccharide structure vibrations [62,63]. On the other hand, the lower intensity of the CS/PEG bands in the green-colored region seem to be more related with the smaller fraction (70%) of CS in that membrane in comparison to that of pure CS one. This supports the hypothesis that the chemical interactions involved in cross-linking occur essentially through the functional groups, as expected, and that skeletal saccharide structure of CS is not participating in those interactions.

The ATR-FTIR spectra of the powders (BCP, CuO and ZnO), and of the membranes without (CS/PEG) and incorporating 1% of each inorganic powder are displayed in **Fig. 7(a)**. The ATR-FTIR spectra of the two membranes are also zoomed in **Fig. 7(b)** to better highlight the effects of the inorganic powders in the chemical cross-linking interactions.

Comparing the spectra of doped and non-doped membranes it can be realized that a significant change occurred in the amide bands. This fact may be related with hydrogen bonds that were developed between amine terminals of CS and dissolved ions of the powders. In acidic media positively charged amine groups are attracted electrostatically by negative charged ions like PO_4^{3-} (from BCP) [64]. These electrostatic forces can lead to the formation of amide bonds

between NH^{3+} and PO_4^{3-}, which justify the deformation in the vibration of amide groups, and, therefore, the change in amide bands.
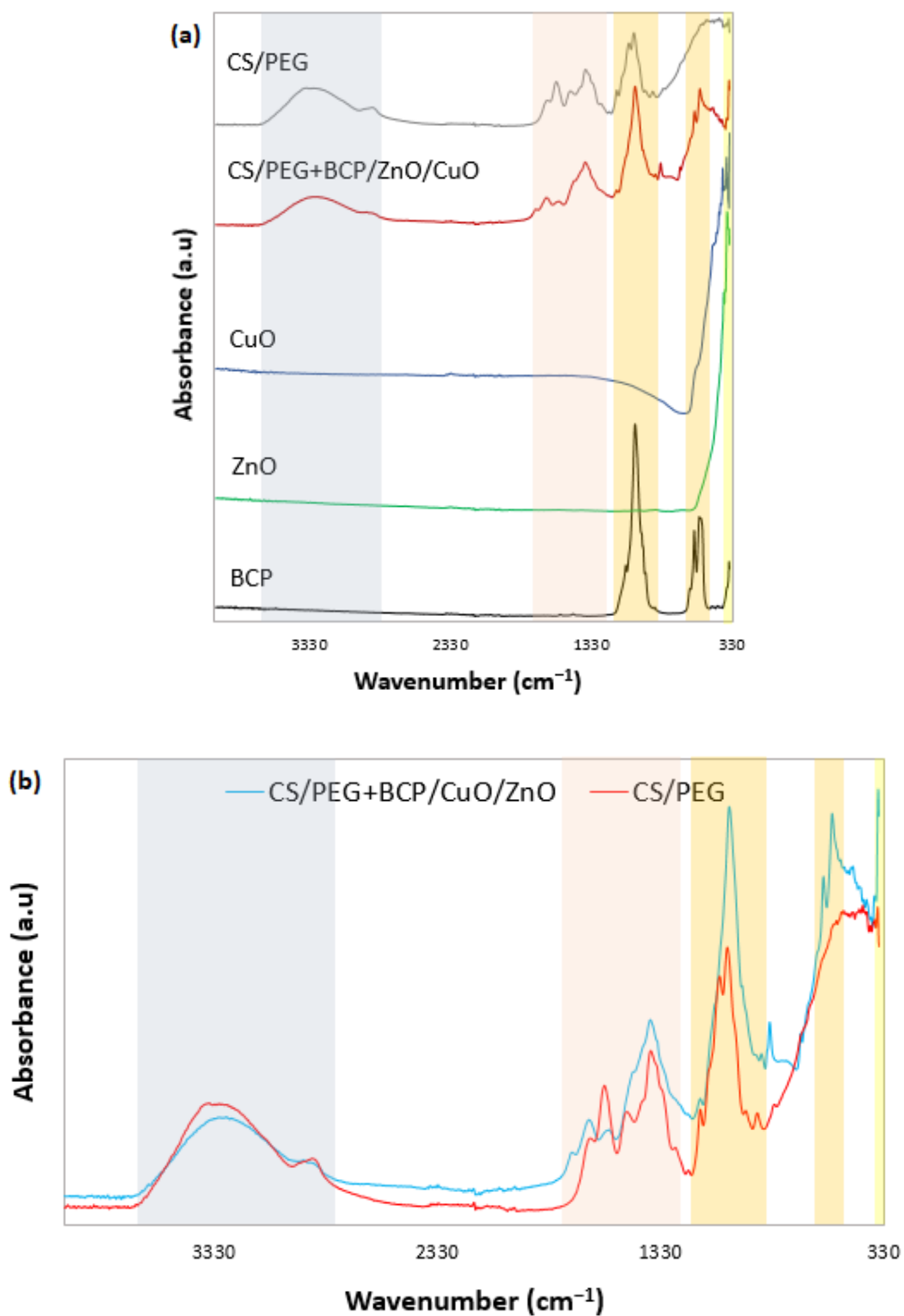

Fig. 7. ATR-FTIR spectra of CS/PEG matrix, composite membrane (1%) and inorganic powders.

Divalent cations such as Ca^{2+}, Cu^{2+} e Zn^{2+} can also bond to phosphate groups by the same electrostatic principle, through the substitution of H^+ ions. The cationic species can bond as well to deprotonated portions that are located in amide and/or hydroxyl groups of the polymer matrix [65]. Inter-chain bridges are then developed, which promote composite cross-linking as suggested in **Fig. 8**.
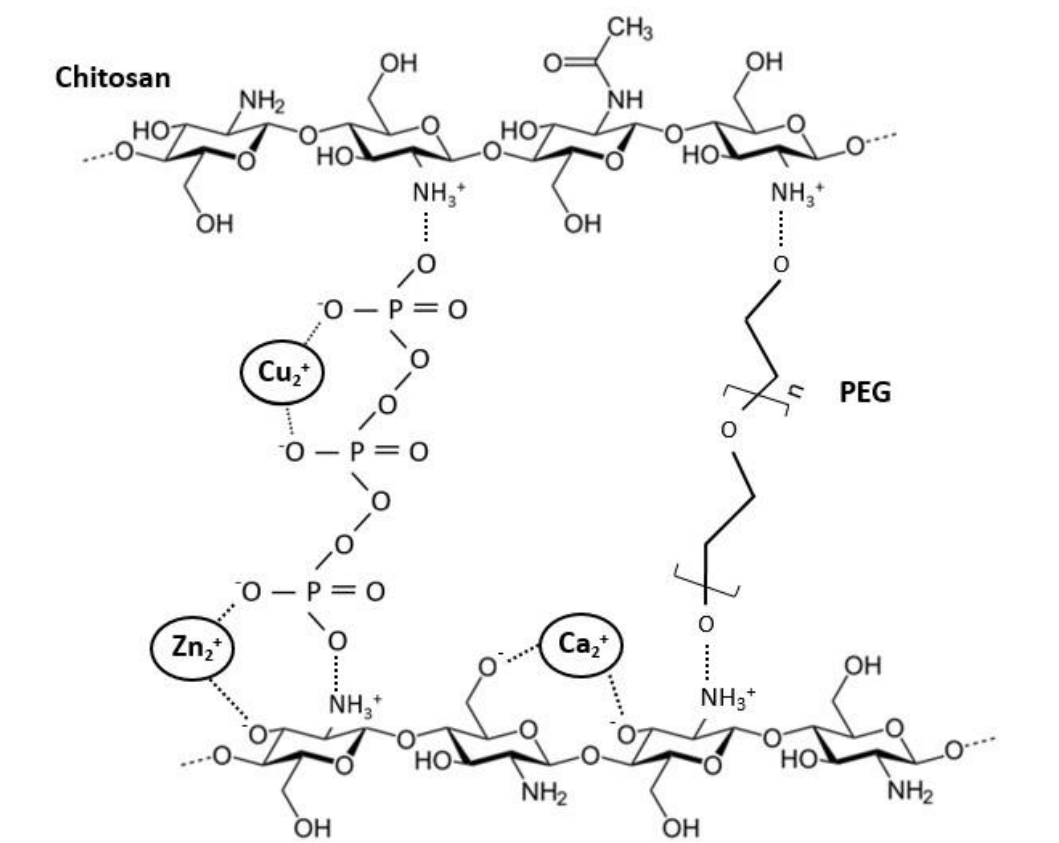

Fig. 8. Schematic representation of the composite cross-linking promoted by the incorporation of BCP, ZnO and CuO particles into the CS/PEG matrix (Adapted from [64–66]).

In the ATR-FTIR spectrum of composite membrane, it is also possible to verify the presence of the characteristic peaks of PO_4^{3-} groups that are present as well in BCP spectrum, at 1010, 559 and 543 cm^{-1} (orange-colored region). ZnO and CuO powders have also their effects on the

composite spectrum, although the corresponding peaks are not so clearly seen by this spectroscopy technique since they are present near to the detection limit, at approximately 354 cm^{-1} (yellow-colored region).

3.3.2. Mechanical evaluation

The relevant mechanical properties of composite membrane (1 %) are compared with those of CS/PEG membrane in **Fig. 9**. Tensile strength at break of doped membrane (2.69 MPa) do not differ significantly from the CS/PEG membrane (2.79 MPa), which means that powders are mainly linked to the polymer matrix and not only dispersed in it. Otherwise, tensile strength of the composite would decrease as the CS/PEG matrix continuity would be interrupted by the inclusion of the particles or agglomerates leading to point defects. Besides, there was a slightly improvement (from 60 % to 72 %) in the elongation capacity of the film with the incorporation of powders, which can be explained by the structural cross-linking between the powders and CS/PEG chains and the gradual relaxation of the composite along the test. The data of mechanical analysis validate the applicability of the composite membranes as coating materials for medical devices.
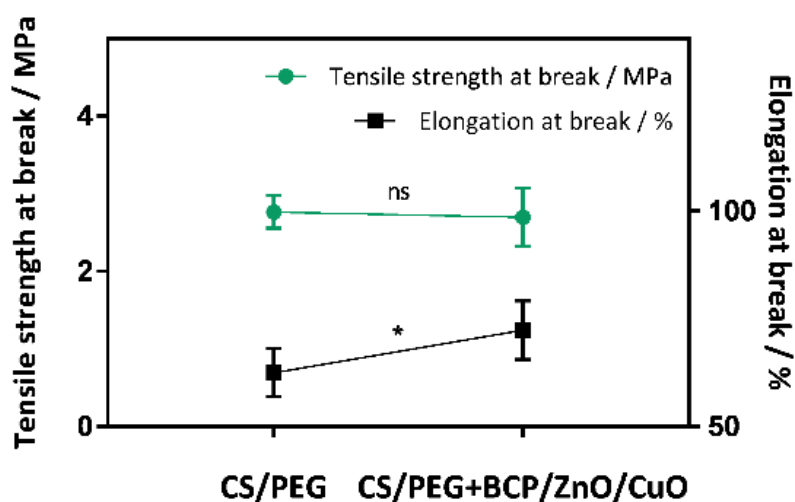
Fig. 9. Mechanical properties comparison between non-doped and doped membranes (ASTM D 882 – 02). The data represent the mean ± SD (n = 5). * stands for $p \leq 0.05$ and "ns" stands for a non-statistically significant difference.

3.3.3. Bioactivity studies

Bioactivity studies in SBF were carried out to evaluate the biodegradability of the composite membranes, and their capacity to promote biomineralization. SEM images of the developed material after each time of immersion in SBF are given in **Fig. 10**. Comparing with non-treated film, after 3 days of incubation there was an increase in the roughness of membrane surface that was gradually softened between 3 days and 14 days. This increase of surface roughness may be associated with the gradual deposition of calcium phosphate particles onto the exposed area of the membrane to SBF. With the continuous particle deposition (3 to 14 days), a uniform apatite layer is then formed, which explains the softening effect. The changes in membrane morphology can also be related with their biodegradation that possibly occurred while biomineralization took place. The biomineralization ability and biodegradation of the composite are highly desirable qualities for bone healing and regeneration.
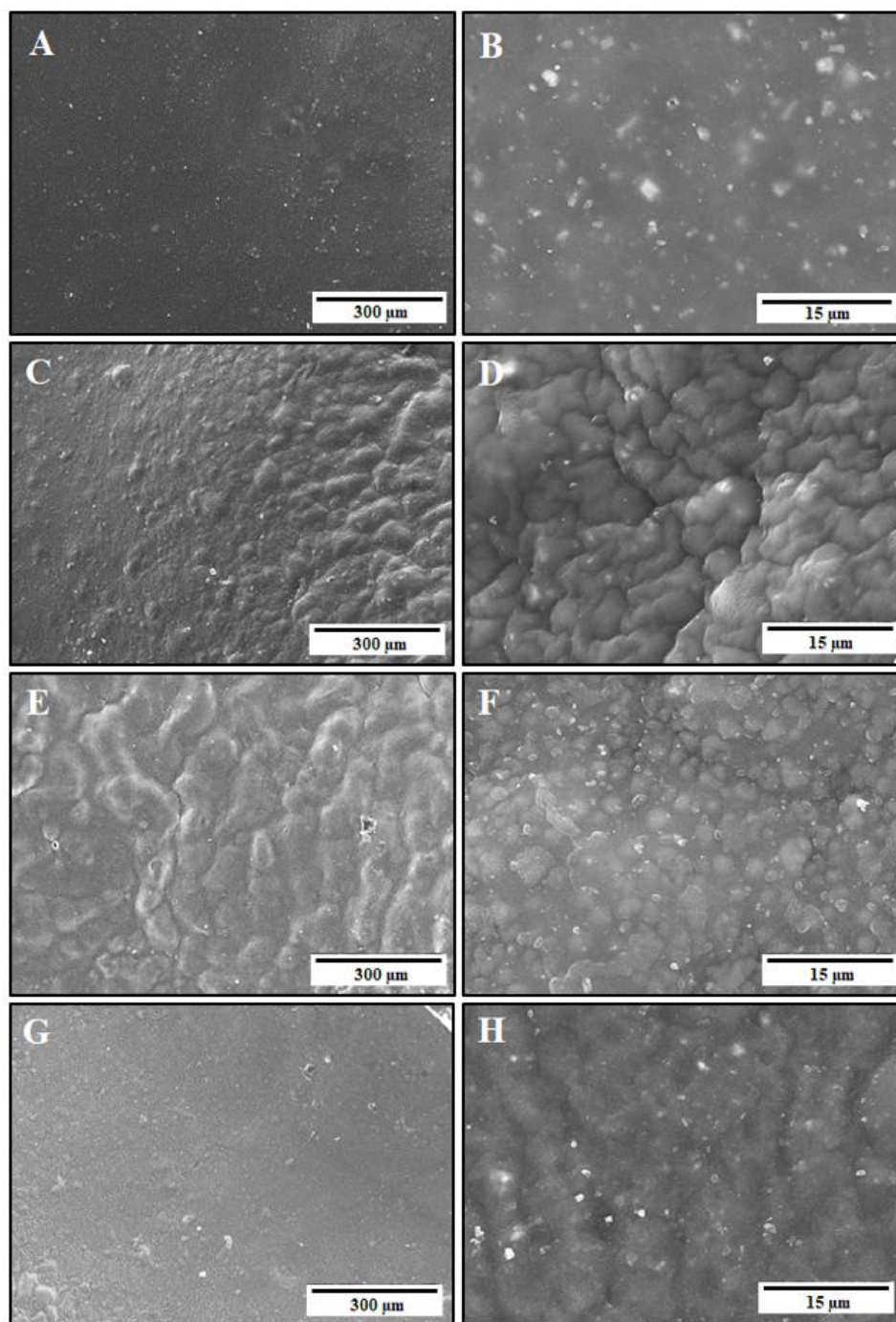
Fig. 10. SEM images of 1 % composite membrane immersed in SBF for: A/B – 0 days; C/D – 3 days; E/F – 7days; and G/H – 14 days.

4.   Conclusion

The present study reports on the fabrication of CS/PEG membranes incorporated with BCP, ZnO and CuO particles. Urea-based hydrothermal treatment of inorganic particles allowed obtaining micro/nanomaterials with a high level of purity and crystallinity. CS/PEG (70/30 %) polymeric matrix was successfully doped via *ex-situ* method with BCP, ZnO and CuO, and the most promising content of metal oxides to be incorporated into the membranes was determined by antibacterial and cytotoxic assays. It was found that the minimum amount of metal oxides that can promote a satisfactory growth inhibition of both Gram-positive *S. aureus* and Gram-negative *E. coli* is 1 % (w/w) of ZnO and CuO. Also, it was proven that membranes doped with up to 1.5 % (w/w) of ZnO and CuO do not induce any cytotoxic effect on Vero cell line. ATR-FTIR analysis revealed that, conceivably, CS amine groups are the main responsible for the composite cross-linking, through the bond that are formed between this protonated terminal and corresponding ions of the powders. The results of the mechanical test also proved that the incorporation of powders into the membranes can enhance its mechanical performance. In short, the selected composite membrane presents a very interesting set of properties, with potential applications in the protection of superficial wounds, in separating soft and hard tissues, and, mainly, as coating material for bone implants, among other applications.

References

[1] D. Campoccia, L. Montanaro, C.R. Arciola, A review of the clinical implications of anti-infective biomaterials andinfection-resistant surfaces, Biomaterials. 34 (2013) 8018–8029. doi:10.1016/j.biomaterials.2013.07.048.

[2] R.K. Singh, S. Awasthi, A. Dhayalan, J.M.F. Ferreira, S. Kannan, Deposition, structure, physical and invitro characteristics of Ag-doped β-Ca3(PO4)2/chitosan hybrid composite coatings on Titanium metal, Mater. Sci. Eng. C. 62 (2016) 692–701. doi:10.1016/j.msec.2016.02.013.

[3] D. Campoccia, L. Montanaro, C.R. Arciola, A review of the biomaterials technologies for infection-resistant surfaces, Biomaterials. 34 (2013) 8533–8554. doi:10.1016/j.biomaterials.2013.07.089.

[4] K. Glinel, P. Thebault, V. Humblot, C.M. Pradier, T. Jouenne, Antibacterial surfaces developed from bio-inspired approaches, Acta Biomater. 8 (2012) 1670–1684. doi:10.1016/j.actbio.2012.01.011.

[5] R.A. Surmenev, M.A. Surmeneva, A.A. Ivanova, Significance of calcium phosphate coatings for the enhancement of new bone osteogenesis - A review, Acta Biomater. 10 (2014) 557–579. doi:10.1016/j.actbio.2013.10.036.

[6] M. Dash, F. Chiellini, R.M. Ottenbrite, E. Chiellini, Chitosan - A versatile semi-synthetic polymer in biomedical applications, Prog. Polym. Sci. 36 (2011) 981–1014. doi:10.1016/j.progpolymsci.2011.02.001.

[7]   R.C.F. Cheung, T.B. Ng, J.H. Wong, W.Y. Chan, Chitosan: An update on potential biomedical and pharmaceutical applications, 2015. doi:10.3390/md13085156.

[8]   I.-Y. Kim, S.-J. Seo, H.-S. Moon, M.-K. Yoo, I.-Y. Park, B.-C. Kim, C.-S. Cho, Chitosan and its derivatives for tissue engineering applications., Biotechnol. Adv. 26 (2008) 1–21. doi:10.1016/j.biotechadv.2007.07.009.

[9]   N. Bhattarai, J. Gunn, M. Zhang, Chitosan-based hydrogels for controlled, localized drug delivery, Adv. Drug Deliv. Rev. 62 (2010) 83–99. doi:10.1016/j.addr.2009.07.019.

[10]   R. Logithkumar, A. Keshavnarayan, S. Dhivya, A. Chawla, S. Saravanan, N. Selvamurugan, A review of chitosan and its derivatives in bone tissue engineering, Carbohydr. Polym. 151 (2016) 172–188. doi:10.1016/j.carbpol.2016.05.049.

[11]   M. Zhang, X.H. Li, Y.D. Gong, N.M. Zhao, X.F. Zhang, Properties and biocompatibility of chitosan films modified by blending with PEG, Biomaterials. 23 (2002) 2641–2648. doi:10.1016/S0142-9612(01)00403-3.

[12]   N.E. Suyatma, L. Tighzert, A. Copinet, V. Coma, Effects of hydrophilic plasticizers on mechanical, thermal, and surface properties of chitosan films, J. Agric. Food Chem. 53 (2005) 3950–3957. doi:10.1021/jf048790+.

[13]   S.K. Mishra, S. Raveendran, J.M.F. Ferreira, S. Kannan, *In Situ* Impregnation of Silver Nanoclusters in Microporous Chitosan-PEG Membranes as an Antibacterial and Drug Delivery Percutaneous Device, Langmuir. (2016) acs.langmuir.6b02844. doi:10.1021/acs.langmuir.6b02844.

[14]   S.K. Mishra, D.S. Mary, S. Kannan, Copper incorporated microporous chitosan-polyethylene glycol hydrogels loaded with naproxen for effective drug release and anti-infection wound dressing, Int. J. Biol. Macromol. 95 (2016) 1–10. doi:10.1016/j.ijbiomac.2016.10.080.

[15] F. Ganji, M.J. Abdekhodaie, Synthesis and characterization of a new thermosensitive chitosan-PEG diblock copolymer, Carbohydr. Polym. 74 (2008) 435–441. doi:10.1016/j.carbpol.2008.03.017.

[16] A. Shavandi, A.E.D.A. Bekhit, M.A. Ali, Z. Sun, M. Gould, Development and characterization of hydroxyapatite/β-TCP/chitosan composites for tissue engineering applications, Mater. Sci. Eng. C. 56 (2015) 481–493. doi:10.1016/j.msec.2015.07.004.

[17] M. Ebrahimi, M.G. Botelho, S. V. Dorozhkin, Biphasic calcium phosphates bioceramics (HA/TCP): Concept, physicochemical properties and the impact of standardization of study protocols in biomaterials research, Mater. Sci. Eng. C. 71 (2017) 1293–1312. doi:10.1016/j.msec.2016.11.039.

[18] Z. Zhang, H. Kurita, H. Kobayashi, K. Kurashina, Osteoinduction with HA/TCP Ceramics of Different Composition and Porous Structure in Rabbits, Oral Sci. Int. 2 (2005) 85–95. doi:10.1016/S1348-8643(05)80011-4.

[19] B. Kundu, A. Lemos, C. Soundrapandian, P.S. Sen, S. Datta, J.M.F. Ferreira, D. Basu, Development of porous HAp and β-TCP scaffolds by starch consolidation with foaming method and drug-chitosan bilayered scaffold based drug delivery system, J. Mater. Sci. Mater. Med. 21 (2010) 2955–2969. doi:10.1007/s10856-010-4127-0.

[20] M. Kucharska, B. Butruk, K. Walenko, T. Brynk, T. Ciach, Fabrication of in-situ foamed chitosan/??-TCP scaffolds for bone tissue engineering application, Mater. Lett. 85 (2012) 124–127. doi:10.1016/j.matlet.2012.07.002.

[21] S. Saravanan, R.S. Leena, N. Selvamurugan, International Journal of Biological Macromolecules Chitosan based biocomposite scaffolds for bone tissue engineering, Int. J. Biol. Macromol. 93 (2016) 1354–1365. doi:10.1016/j.ijbiomac.2016.01.112.

[22]   D. Wawro, L. Pighinelli, Chitosan fibers modified with HAp/??-TCP nanoparticles, Int. J. Mol. Sci. 12 (2011) 7286–7300. doi:10.3390/ijms12117286.

[23]   M.R. Nikpour, S.M. Rabiee, M. Jahanshahi, Synthesis and characterization of hydroxyapatite/chitosan nanocomposite materials for medical engineering applications, Compos. Part B Eng. 43 (2012) 1881–1886. doi:10.1016/j.compositesb.2012.01.056.

[24]   M. Li, Q.-F. Ke, S.-C. Tao, S.-C. Guo, B.-Y. Rui, Y.-P. Guo, Fabrication of hydroxyapatite/chitosan composite hydrogels loaded with exosomes derived from miR-126-3p overexpressed synovial mesenchymal stem cells for diabetic chronic wound healing, J. Mater. Chem. B. 4 (2016) 6830–6841. doi:10.1039/C6TB01560C.

[25]   A. Tripathi, S. Saravanan, S. Pattnaik, A. Moorthi, N.C. Partridge, N. Selvamurugan, Bio-composite scaffolds containing chitosan/nano-hydroxyapatite/nano-copper-zinc for bone tissue engineering, Int. J. Biol. Macromol. 50 (2012) 294–299. doi:10.1016/j.ijbiomac.2011.11.013.

[26]   P. Rajasekaran, S. Santra, Hydrothermally Treated Chitosan Hydrogel Loaded with Copper and Zinc Particles as a Potential Micronutrient-Based Antimicrobial Feed Additive, Front. Vet. Sci. 2 (2015) 1–9. doi:10.3389/fvets.2015.00062.

[27]   F. Wahid, J.J. Yin, D.D. Xue, H. Xue, Y.S. Lu, C. Zhong, L.Q. Chu, Synthesis and characterization of antibacterial carboxymethyl Chitosan/ZnO nanocomposite hydrogels, Int. J. Biol. Macromol. 88 (2016) 273–279. doi:10.1016/j.ijbiomac.2016.03.044.

[28]   H. Zazo, C.I. Colino, J.M. Lanao, Current applications of nanoparticles in infectious diseases, J. Control. Release. 224 (2016) 86–102. doi:10.1016/j.jconrel.2016.01.008.

[29]   V. Graziani, M. Fosca, A.A. Egorov, Y. V. Zobkov, A.Y. Fedotov, A.E. Baranchikov, M. Ortenzi, R. Caminiti, V.S. Komlev, J. V. Rau, Zinc-releasing calcium phosphate cements for

bone substitute materials, Ceram. Int. 42 (2016) 17310–17316. doi:10.1016/j.ceramint.2016.08.027.

[30] G. Fielding, S. Bose, SiO2 and ZnO dopants in three-dimensionally printed tricalcium phosphate bone tissue engineering scaffolds enhance osteogenesis and angiogenesis in vivo, Acta Biomater. 9 (2013) 9137–9148. doi:10.1016/j.actbio.2013.07.009.

[31] S.M. Dizaj, F. Lotfipour, M. Barzegar-Jalali, M.H. Zarrintan, K. Adibkia, Antimicrobial activity of the metals and metal oxide nanoparticles, Mater. Sci. Eng. C. 44 (2014) 278–284. doi:10.1016/j.msec.2014.08.031.

[32] P. Mantecca, E. Moschini, P. Bonfanti, U. Fascio, I. Perelshtein, A. Lipovsky, G. Chirico, R. Bacchetta, L. Del Giacco, A. Colombo, A. Gedanken, Toxicity evaluation of a new Zn-doped CuO nanocomposite with highly effective antibacterial properties, Toxicol. Sci. 146 (2015) 16–30. doi:10.1093/toxsci/kfv067.

[33] E. Malka, I. Perelshtein, A. Lipovsky, Y. Shalom, L. Naparstek, N. Perkas, T. Patick, R. Lubart, Y. Nitzan, E. Banin, A. Gedanken, Eradication of multi-drug resistant bacteria by a novel Zn-doped CuO nanocomposite, Small. 9 (2013) 4069–4076. doi:10.1002/smll.201301081.

[34] Z. Mohammadi, A. Sheikh-Mehdi Mesgar, F. Rasouli-Disfani, Preparation and characterization of single phase, biphasic and triphasic calcium phosphate whisker-like fibers by homogenous precipitation using urea, Ceram. Int. 42 (2015) 6955–6961. doi:10.1016/j.ceramint.2016.01.081.

[35] K. Ada, M. Gökgöz, M. Önal, Y. Sarikaya, Preparation and characterization of a ZnO powder with the hexagonal plate particles, Powder Technol. 181 (2008) 285–291. doi:10.1016/j.powtec.2007.05.015.

[36] Y. Wang, J. Wang, H. Chen, M. Yao, Y. Li, Preparation and NOx-assisted soot oxidation activity of a CuO-CeO2 mixed oxide catalyst, Chem. Eng. Sci. 135 (2015) 294–300. doi:10.1016/j.ces.2015.03.024.

[37] C.K. Srikanth, P. Jeevanandam, Effect of anion on the homogeneous precipitation of precursors and their thermal decomposition to zinc oxide, J. Alloys Compd. 486 (2009) 677– 684. doi:10.1016/j.jallcom.2009.07.031.

[38] A.B. Moghaddam, M. Moniri, S. Azizi, R.A. Rahim, A. Bin Ariff, W.Z. Saad, F. Namvar, M. Navaderi, R. Mohamad, Biosynthesis of ZnO nanoparticles by a new Pichia kudriavzevii yeast strain and evaluation of their antimicrobial and antioxidant activities, Molecules. 22 (2017). doi:10.3390/molecules22060872.

[39] R. Pati, R.K. Mehta, S. Mohanty, A. Padhi, M. Sengupta, B. Vaseeharan, C. Goswami, A. Sonawane, Topical application of zinc oxide nanoparticles reduces bacterial skin infection in mice and exhibits antibacterial activity by inducing oxidative stress response and cell membrane disintegration in macrophages, Nanomedicine Nanotechnology, Biol. Med. 10 (2014) 1195–1208. doi:10.1016/j.nano.2014.02.012.

[40] A.C. Jayasuriya, A. Aryaei, A.H. Jayatissa, ZnO nanoparticles induced effects on nanomechanical behavior and cell viability of chitosan films, Mater. Sci. Eng. C. 33 (2013) 3688–3696. doi:10.1016/j.msec.2013.04.057.

[41] H. Alishah, S. Pourseyedi, S.Y. Ebrahimipour, S.E. Mahani, N. Rafiei, Green synthesis of starch-mediated CuO nanoparticles: preparation, characterization, antimicrobial activities and in vitro MTT assay against MCF-7 cell line, Rend. Lincei. 28 (2017) 65–71. doi:10.1007/s12210-016-0574-y.

[42] R. Chakraborty, R.K. Sarkar, A.K. Chatterjee, U. Manju, A.P. Chattopadhyay, T. Basu, A simple, fast and cost-effective method of synthesis of cupric oxide nanoparticle with

promising antibacterial potency: Unraveling the biological and chemical modes of action, Biochim. Biophys. Acta - Gen. Subj. 1850 (2015) 845–856. doi:10.1016/j.bbagen.2015.01.015.

[43]   M. Ahamed, H.A. Alhadlaq, M.A.M. Khan, P. Karuppiah, N.A. Al-dhabi, Synthesis , Characterization , and Antimicrobial Activity of Copper Oxide Nanoparticles, J. Nanomater. 2014 (2014) 1–4. doi:10.1155/2014/637858.

[44]   A. E2149-13a, Standard Test Method for Determining the Antimicrobial Activity of Immobilized Antimicrobial Agents Under Dynamic Contact Conditions, (2013) 11–14. doi:10.1520/E2149-10.Copyright.

[45]   I. Standard, International Organization for Standardization. ISO 10993-5, Biol. Eval. Med. Devices- Tests Vitr. Cytotox. 2009 (2009) 34. doi:10.1081/E-ELIS3-120044716.

[46]   Ammerman, Growth and Maintenance of Vero Cell Lines, Curr Protoc Microbiol. (2009) 1–10. doi:10.1002/9780471729259.mca04es11.Growth.

[47]   A. American, N. Standard, Standard Test Method for Tensile Properties of Thin Plastic Sheeting, 14 (2002) 1–11.

[48]   J.S. a W. Store, INTERNATIONAL STANDARD evaluation for apatite-forming ability, 2012 (2012).

[49]   A.C. Popa, G.E. Stan, M.A. Husanu, I. Mercioniu, L.F. Santos, H.R. Fernandes, J.M.F. Ferreira, Bioglass implant-coating interactions in synthetic physiological fluids with varying degrees of biomimicry, Int. J. Nanomedicine. 12 (2017) 683–707. doi:10.2147/IJN.S123236.

[50]   S. Lala, B. Satpati, S.K. Pradhan, Sintering behavior and growth mechanism of β-TCP in nanocrystalline hydroxyapatite synthesized by mechanical alloying, Ceram. Int. 42 (2016) 13176–13182. doi:10.1016/j.ceramint.2016.05.109.

[51] Y. Zhang, J. Lu, S. Yang, Preparation of hydroxyapatite ceramic through centrifugal casting process using ultra-fine spherical particles as precursor and its decomposition at high temperatures, J. Adv. Ceram. 1 (2012) 60–65. doi:10.1007/s40145-012-0006-0.

[52] K. Sowri Babu, A. Ramachandra Reddy, C. Sujatha, K. Venugopal Reddy, A.N. Mallika, Synthesis and optical characterization of porous ZnO, J. Adv. Ceram. 2 (2013) 260–265. doi:10.1007/s40145-013-0069-6.

[53] K. Phiwdang, S. Suphankij, W. Mekprasart, W. Pecharapa, Synthesis of CuO nanoparticles by precipitation method using different precursors, Energy Procedia. 34 (2013) 740–745. doi:10.1016/j.egypro.2013.06.808.

[54] F.A. Corsello, P.A. Bolla, P.S. Anbinder, M.A. Serradell, J.I. Amalvy, P.J. Peruzzo, Morphology and properties of neutralized chitosan-cellulose nanocrystals biocomposite films, Carbohydr. Polym. 156 (2017) 452–459. doi:10.1016/j.carbpol.2016.09.031.

[55] A. Sirelkhatim, S. Mahmud, A. Seeni, N.H.M. Kaus, L.C. Ann, S.K.M. Bakhori, H. Hasan, D. Mohamad, Review on zinc oxide nanoparticles: Antibacterial activity and toxicity mechanism, Nano-Micro Lett. 7 (2015) 219–242. doi:10.1007/s40820-015-0040-x.

[56] W. Jiang, A. Saxena, B. Song, B.B. Ward, T.J. Beveridge, S.C.B. Myneni, Elucidation of functional groups on gram-positive and gram-negative bacterial surfaces using infrared spectroscopy, Langmuir. 20 (2004) 11433–11442. doi:10.1021/la049043+.

[57] N. Bala, M. Sarkar, M. Maiti, P. Nandy, R. Basu, S. Das, Phenolic compound-mediated single-step fabrication of copper oxide nanoparticles for elucidating their influence on anti-bacterial and catalytic activity, New J. Chem. 41 (2017) 4458–4467. doi:10.1039/C6NJ04008J.

[58] K. Poole, Efflux pumps as antimicrobial resistance mechanisms, Ann. Med. 39 (2007) 162–

176.

[59] M. Putman, W. Hendrik, Molecular Properties of Bacterial Multidrug Transporters, 64 (2000) 672–693.

[60] Z. Jaglic, D. Cervinkova, Genetic basis of resistance to quaternary ammonium compounds – the qac genes and their role : a review, 2012 (2012) 275–281.

[61] J.D.Æ.Y. Hsieh, PEGylation of chitosan for improved solubility and fiber formation via electrospinning PEGylation of chitosan for improved solubility and fiber formation via electrospinning, (2014). doi:10.1007/s10570-007-9122-3.

[62] T. Buranachai, N. Praphairaksit, N. Muangsin, Chitosan/Polyethylene Glycol Beads Crosslinked with Tripolyphosphate and Glutaraldehyde for Gastrointestinal Drug Delivery, AAPS PharmSciTech. 11 (2010) 1128–1137. doi:10.1208/s12249-010-9483-z.

[63] M. Bin Ahmad, M.Y. Tay, K. Shameli, M.Z. Hussein, J.J. Lim, Green synthesis and characterization of silver/chitosan/polyethylene glycol nanocomposites without any reducing agent, Int. J. Mol. Sci. 12 (2011) 4872–4884. doi:10.3390/ijms12084872.

[64] S.T. Lee, F.L. Mi, Y.J. Shen, S.S. Shyu, Equilibrium and kinetic studies of copper (II) ion uptake by chitosan-tripolyphosphate chelating resin, Polymer (Guildf). 42 (2001) 1879–1892.

[65] G.Z. Kyzas, E.A. Deliyanni, Mercury(II) removal with modified magnetic chitosan adsorbents, Molecules. 18 (2013) 6193–6214. doi:10.3390/molecules18066193.

[66] Y. Cai, L. Zheng, Z. Fang, Selective adsorption of Cu(II) from an aqueous solution by ion imprinted magnetic chitosan microspheres prepared from steel pickling waste liquor, RSC Adv. 5 (2015) 97435–97445. doi:10.1039/c5ra16547d.
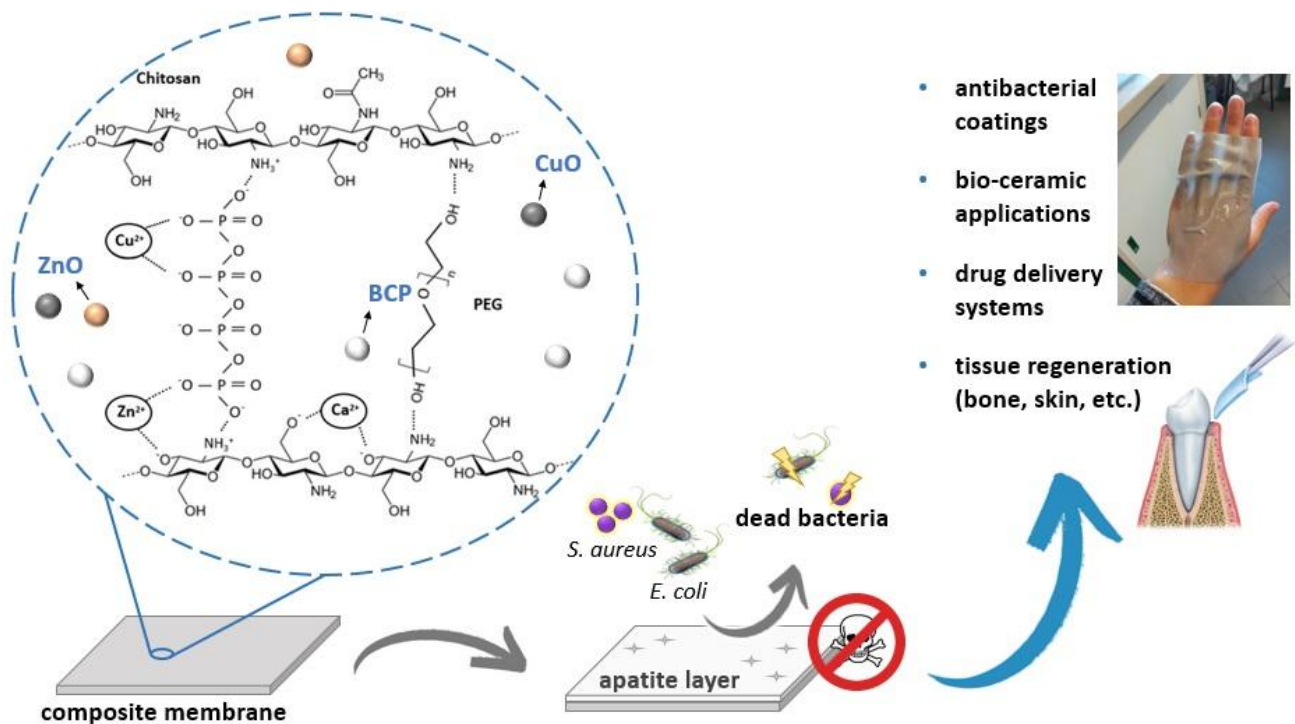
Graphical abstract

Highlights

- Composite Chitosan/Polyethylene glycol matrix membranes with functional particles.

- Biphasic calcium phosphates for bioactivity; ZnO and CuO with bactericidal roles.

- Membranes doped with 1% of each metal oxide exhibit bacteriostatic activity.

- Adding up to 1.5% of ZnO and CuO does not induce cytotoxicity on Vero cells.

- Inorganic particles enhanced cross-linking and flexibility of membranes.

- Growth of apatite layer was observed after 3rd days of immersion in SBF.